AGU PUBLICATIONS

Global Biogeochemical Cycles

RESEARCH ARTICLE
10.1002/2016GB005614

Key Points:
- Surface biogeochemical properties show highly significant relationships to depth integrals, which provides the ability to extrapolate satellite data vertically
- The explained variance in these relationships decreases as subsurface maxima become more pronounced
- Coccolithophores, coccoliths, and PIC show highest integrated concentrations at moderate stratification levels at the base of the euphotic zone

Correspondence to:
W. M. Balch,
bbalch@bigelow.org

Citation:
Balch, W. M., Bowler, B. C., Drapeau, D. T., Lubelczyk, L. C., & Lyczkowski, E. (2018). Vertical distributions of coccolithophores, PIC, POC, biogenic silica, and chlorophyll *a* throughout the global ocean. *Global Biogeochemical Cycles*, *32*, 2–17. https://doi.org/10.1002/2016GB005614

Received 23 DEC 2016
Accepted 10 DEC 2017
Accepted article online 14 DEC 2017
Published online 9 JAN 2018

Vertical Distributions of Coccolithophores, PIC, POC, Biogenic Silica, and Chlorophyll *a* Throughout the Global Ocean

William M. Balch[1], Bruce C. Bowler[1], David T. Drapeau[1], Laura C. Lubelczyk[1], and Emily Lyczkowski[1]

[1]Bigelow Laboratory for Ocean Sciences, East Boothbay, ME, USA

Abstract Coccolithophores are a critical component of global biogeochemistry, export fluxes, and seawater optical properties. We derive globally significant relationships to estimate integrated coccolithophore and coccolith concentrations as well as integrated concentrations of particulate inorganic carbon (PIC) from their respective surface concentration. We also examine surface versus integral relationships for other biogeochemical variables contributed by all phytoplankton (e.g., chlorophyll *a* and particulate organic carbon) or diatoms (biogenic silica). Integrals are calculated using both 100 m integrals and euphotic zone integrals (depth of 1% surface photosynthetically available radiation). Surface concentrations are parameterized in either volumetric units (e.g., m^{-3}) or values integrated over the top optical depth. Various relationships between surface concentrations and integrated values demonstrate that when surface concentrations are above a specific threshold, the vertical distribution of the property is biased to the surface layer, and when surface concentrations are below a specific threshold, the vertical distributions of the properties are biased to subsurface maxima. Results also show a highly predictable decrease in explained-variance as vertical distributions become more vertically heterogeneous. These relationships have fundamental utility for extrapolating surface ocean color remote sensing measurements to 100 m depth or to the base of the euphotic zone, well beyond the depths of detection for passive ocean color remote sensors. Greatest integrated concentrations of PIC, coccoliths, and coccolithophores are found when there is moderate stratification at the base of the euphotic zone.

Plain Language Summary We use a global shipboard data set to describe the vertical distributions of coccolithophores (marine phytoplankton that produce microscopic calcium carbonate scales). These plants are responsible for over half of all the suspended calcium carbonate in the ocean, they can cause major increases in water reflectance in blooms spanning entire ocean basins, and they provide ballast to organic matter to the deep sea and thus are strong drivers of the ocean's biological carbon pump (responsible for sequestering carbon in the deep sea). This paper describes global relationships that relate the surface concentrations of coccolithophores and their particulate inorganic carbon (as observed by satellite) to concentrations found over the upper 100 m of the ocean or the entire euphotic zone. These predictions function from highest productivity waters to the lowest productivity, "biological deserts" in the sea. We also include predictive relationships for biogeochemical variables related to other phytoplankton groups (e.g., diatoms) as well as more generic indicators of phytoplankton (e.g., chlorophyll and particulate organic carbon). The results provide new oceanographic insights into the ecology and biogeochemistry of these microalgal groups.

1. Introduction

Coccolithophores are ubiquitous marine nanoalgae belonging to the class Prymnesiophyceae (within the division Haptophyta) that produce external scales, some of which exist as calcite plates called coccoliths (Billard & Inouye, 2004; Edvardsen et al., 2000). Calcifying, plated coccolithophore cells and their detached coccoliths are profoundly important: to marine optics (because of their intense light scattering properties) (Holligan et al., 1983), to biogeochemistry (because of their density and strong ballasting of particulate organic matter, a major driver of the ocean biological carbon pump) (Francois et al., 2002), to carbon cycling (because of the biochemistry of calcite formation, which produces a molecule of CO_2 for every molecule of $CaCO_3$ produced) (Robertson et al., 1994), and to microbial ecology (where coccolithophores are frequent competitors with other classes of phytoplankton). This competition has traditionally been thought to hinge on balances of nutrients and turbulence (Margalef, 1978), which fundamentally affects the export of particulate organic carbon (POC) and particulate inorganic carbon (PIC) from the euphotic zone of (Balch et al., 2010).

Coccolithophores inhabit a wide variety of depths within the euphotic zone (and aphotic zone), largely a function of their ecological preferences. Dense, highly reflective blooms of the coccolithophore, *Emiliania huxleyi* are generally confined to temperate to subpolar waters in the upper part of the euphotic zone (Balch et al., 1996, 2016; Brown & Yoder, 1994; Holligan et al., 2010; Hopkins et al., 2015; Poulton et al., 2010) while the more diverse assemblages in subtropical and tropical realms are spread much more uniformly over the euphotic zone (McIntyre & Be, 1967; Reid, 1980). However, the passive remote sensing of coccolithophore PIC (as well as phytoplankton chlorophyll in general) is strongly biased to the top optical depth (~37% light level) of the water column (Gordon & McCluney, 1975), which presents a major problem for their detection over the entire euphotic zone. This is especially true in warm tropical and subtropical waters where coccolithophores can be found as deep as the 0.1% light level (Poulton et al., 2017).

Coccolithophore PIC can be detected using space-based ocean color remote sensing. The NASA ocean color PIC algorithm represents a merging of two different published PIC algorithms: a two-band algorithm (Balch et al., 2005), which works optimally in waters with low suspended $CaCO_3$ concentrations (applicable to ~95% of the time and space in the surface ocean where PIC concentrations are $<$0.003 mol m^{-3}) and a three-band, red/near infrared algorithm, which performs best at higher $CaCO_3$ concentrations (Gordon et al., 2001) and is less affected by colored dissolved organic matter. Both algorithms are fundamentally based on predicting particle backscattering of PIC and subsequent conversion of this to PIC concentration based on an average backscattering cross section of coccolithophore PIC. Since the original inception of the merged PIC algorithm, it has been used for a wide variety of applications (Balch et al., 2007; Freeman & Lovenduski, 2015; Galí et al., 2015; Hopkins et al., 2015).

The phytoplankton variable that has received the most attention relevant to its vertical distribution is chlorophyll *a*. The presence of a subsurface chlorophyll maximum was first documented by Strickland (1968) in the Southern California Bight. He showed that the chlorophyll maximum typically occurs above the 1% light depth (the traditional definition of the base of the euphotic zone), which also frequently is co-located near the nitracline. Chlorophyll fluorescence maxima are frequently maxima in extractable-chlorophyll concentration, and these are frequently (but not always) maxima in phytoplankton biomass (Cullen & Eppley, 1981). The mechanisms of formation of the subsurface chlorophyll maxima can be related to hydrography, behavior, algal growth, and physiology (Cullen, 1982). Subsurface peaks in the vertical profiles of other biogeochemical variables have received minimal attention regarding their global trends.

For determining integrated phytoplankton chlorophyll concentration, the solution over the last several decades has been to use statistical means to estimate the euphotic concentration of chlorophyll based on satellite-derived, surface chlorophyll in the top optical depth (Balch et al., 1992; Morel, 1988; Platt et al., 1988; Platt & Herman, 1983). However, now there are passive remote sensing algorithms for other biogeochemical properties such as POC (which includes both living POC of autotrophs and heterotrophs as well as detrital POC) (Stramski et al., 2008), biogenic silica (BSi) (Balch et al., 2010) and PIC (which technically can include other PIC particles than coccoliths) (Balch et al., 2005; Gordon et al., 2001). It is not currently appreciated if there is statistically significant vertical structure with subsurface maxima for coccolithophores, their detached coccoliths, PIC, or, for that matter, other biogeochemical properties such as POC and BSi, as there is for chlorophyll (Cullen, 1982). If one could statistically derive their integrated concentration based on surface satellite measurements, then this would have a major impact on the fields of ocean remote sensing and global ocean biogeochemistry. In this paper, we use a global data set consisting of $>$1,300 stations from all the major oceans to assess the vertical structure of these biogeochemically relevant variables and to assess whether there are any unifying relationships that can be used to improve the accuracy of 100 m or euphotic-integrated estimates of these materials using passive, space-based ocean color measurements (representative of only surface waters).

2. Methods

2.1. Regions Sampled and Water Sampling Protocols

The data to be presented in this paper were collected on 17 cruises between July 1995 and November 2012, which occurred in all major oceans, including the Southern Ocean and Arctic Ocean (Table 1 and Figure 1). The data set has an Atlantic Ocean bias since we include eight Atlantic Meridional Transect cruises between the United Kingdom and either South Africa or southern Chile (or the Falkland Islands). Sampling over the

Table 1
Specific Cruise Details (Ship, Location, Number of Stations, and Underway Samples (UW) and Dates) for Data Used in This Work

Cruise	Ship	Sampling domain	# Stn profiles	# Surf. UW samples	Date first Stn	Date last Stn	# Sample days
JGOFS Arabian Sea P04-Monsoon	R/V *Thompson*	Arabian Sea, Indian Ocean	19	19	18/7/1995	13/8/1995	27
JGOFS Arabian Sea P06-Intermonsoon	R/V *Thompson*	Arabian Sea, Indian Ocean	5	17	29/10/1995	23/11/1995	26
Atlantic Meridional Transect '15	*RRS Discovery*	North and South Atlantic Ocean	63	112	19/9/2004	26/10/2004	38
EqPac'04-Biocomplexity	R/V *Revelle*	Equatorial Pacific (110°-140°W)	11	7	10/12/2004	28/12/2004	19
Atlantic Meridional Transect '16	*RRS Discovery*	North and South Atlantic Ocean	53	131	21/5/2005	26/6/2005	37
EqPac'05-Biocomplexity	R/V *Revelle*	Equatorial Pacific (123°-140°W)	15	0	7/9/2005	23/9/2005	17
Atlantic Meridional Transect '17	*RRS Discovery*	North and South Atlantic Ocean	52	175	18/10/2005	26/11/2005	40
Atlantic Meridional Transect '18	*RRS James Clark Ross*	North and South Atlantic Ocean	51	111	4/10/2008	8/11/2008	36
COPAS'08	R/V *Revelle*	Patagonian Shelf, Atlantic Ocean	33	54	5/12/2008	31/12/2008	27
Atlantic Meridional Transect '19	*RRS James Cook*	North and South Atlantic Ocean	67	110	14/10/2009	27/11/2009	45
Atlantic Meridional Transect '20	*RRS James Cook*	North and South Atlantic Ocean	60	134	13/10/2010	22/11/2010	41
Great Belt-I	R/V *Melville*	Southern Ocean-Atlantic Sector	31	91	13/1/2011	13/2/2011	32
Tangaroa'11	R/V *Tangaroa*	SW Subtropical Pacific Ocean	18	29	9/6/2011	28/6/2011	20
ICESCAPE'11	R/V *Healy*	Western Arctic/Chukchi Sea	16	90	28/6/2011	24/7/2011	27
Atlantic Meridional Transect '21	*RRS Discovery*	North and South Atlantic Ocean	68	94	30/9/2011	9/11/2011	41
Great Belt-II	R/V *Revelle*	Southern Ocean-Indian Sector	32	92	20/2/2012	20/3/2012	30
Atlantic Meridional Transect '22	*RRS James Cook*	North and South Atlantic Ocean	67	90	11/10/2012	20/11/2012	41
Total			661	1356			544

water column used a conductivity-temperature-depth (CTD) rosette with typically 6–8 Niskin bottles tripped within the euphotic zone (roughly down to the 0.1% light depth). The percent light estimates were based either on a PAR light sensor on the CTD (during daylight hours as compared to a surface reference) or at night, the profile of beam attenuation ($c(\lambda)$ where λ denotes wavelength), used to predict spectral downwelling diffuse attenuation ($K_d(\lambda)$) (Balch et al., 2011) and associated percent light estimates. Discrete surface samples were also regularly drawn from the ships' underway seawater lines for calibration and validation of the underway sampling system.

2.2. Discrete Sample Analyses

The technique of Poulton et al. (2006) was used to measure $CaCO_3$ concentration. Briefly, 100–200 mL samples were filtered onto 0.4 μm pore size polycarbonate filters then rinsed with potassium tetraborate buffer (adjusted to pH = 8) to remove seawater calcium chloride. This pH adjustment was critical to insure that carbonates were stable during sample storage. Later, filters were dried at 60°C, placed in trace metal-free

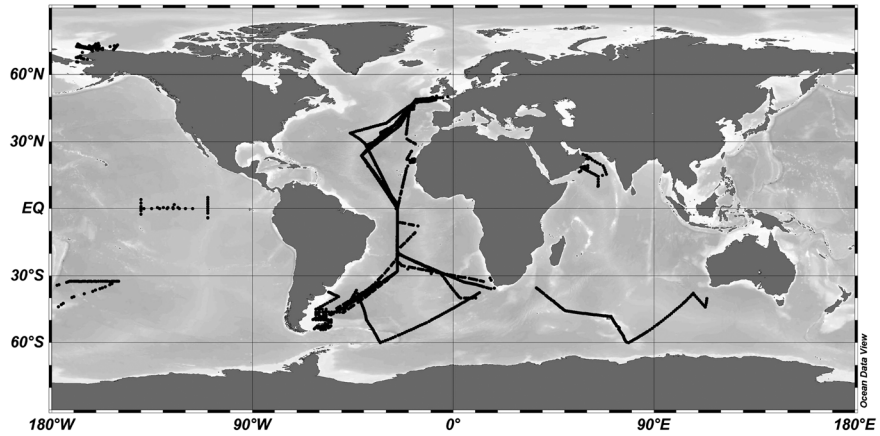

Figure 1. Map of station locations for data used in this study. See Table 1 for specific cruise details. The gray shading of the global oceans represents relative depth (lighter regions are shallower).

centrifuge tubes with 5 mL 0.5% Optima grade nitric acid and the Ca concentration measured using inductively coupled plasma-optical emission spectroscopy (Cheng et al., 2004). Chlorophyll and particulate organic carbon samples were filtered through 0.45 μm pore size nitrocellulose HA filters and baked GF/F filters, respectively, and measured according to the JGOFS protocols (JGOFS, 1996). Note that the JGOFS protocols call for GF/F filters for chlorophyll analysis but 0.45 μm pore size nitrocellulose HA filters have higher efficiencies of capture than GF/F filters, particularly for picoplankton size fractions (Phinney & Yentsch, 1985). BSi was measured using 0.4 μm poresize polycarbonate filters and the NaOH digestion technique (Brzezinski & Nelson, 1989), which is based on the original technique of Paasche (1973). The technique dissolves >98% of the amorphous (biogenic) silica and <1% of the mineral silica, after which the reactive silicate was analyzed (Parsons et al., 1984). Microscope enumeration of coccolithophores and coccoliths (for total abundance) was performed by filtering a 50–100 mL water sample through a Millipore HA filter, rinsed with potassium tetraborate buffer, and frozen in a petri dish until counted (Haidar et al., 2000; Haidar & Thierstein, 2001). Prior to mounting of filters, they were dried in an oven at 60°C. *Canada* Balsam (60°C) or Norland brand optical adhesive was first placed on top of a cleaned microscope slide, then the sample filter was placed on top of this, followed by a cover slip. The clarified filter was examined with an Olympus BH2 microscope equipped with polarization optics and automated sample stage after which birefringent coccoliths and plated coccolithophores were imaged for counting. For statistical reasons, at least 150 microscope fields were imaged. Coccoliths and plated coccolithophore images were processed with CCC image-analysis software (Balch & Utgoff, 2009).

CCC software cannot distinguish between coccospheres and coccolith aggregates since, when using polarized microscopy only, the birefringence is viewed against a dark background and cellular detail is not visible. Moreover, even using unpolarized, transmitted light microcsopy, specimens viewed through an HA filter mounted on a glass slide with optical adhesive are still not completely transparent and cellular detail is not visible. Therefore, we only report the total of plated coccolithophores and coccolith aggregates in this work. Nonetheless, as there is considerable birefringent debris in ocean water, polarization microscopy remains a fast, reliable way to discriminate that debris from coccoliths or plated cells (Balch & Fabry, 2008) (note that the latter have distinct birefringence patterns that CCC uses to aid in identification; Moshkovitz & Osmond, 1989). Water column integration of all variables used standard trapezoidal integration.

2.3. Determining Homogeneity or Heterogeneity for Various Vertical Properties

For optimal application of these measurements to remote sensing, we first analyzed the relationship between the 100 m integrated values of the various properties (*Y* axis) versus the shallowest value of the property in the top 10 m (*X* axis; which, in most cases in oceanic waters, will represent the concentration in the top optical depth observed in ocean color satellites) (Gordon & McCluney, 1975). For our analysis of 100 m integrated versus surface concentrations of various properties, if a property was homogenously distributed over 100 m, then a plot of 100 m integrated value versus surface concentration would have a slope of 100 m^{-1} (i.e., 100X the surface value; we henceforth call this the "homogeneity line"). If there was a maximum in a subsurface property, not reflected in the surface water sample, then the ratio of the integrated concentration to surface concentration would be greater than 100 m^{-1}. Conversely, if there was a surface peak in concentration, greater than the subsurface concentrations (integrated down to 100 m depth), then the ratio of integrated values to surface values would be <100 m^{-1}. Thus, all resultant plots for the global data set show the 100 m integrated concentration plotted against the surface concentration, with the homogeneous distribution (homogeneity line with slope100 m^{-1}) shown as a dashed line for reference.

We also calculated the integrated euphotic zone concentrations and compared this to the surface concentration (as above) or the concentration integrated over the top optical depth. The euphotic zone was defined as the depth where the downwelling irradiance (as photosynthetically available radiation (PAR) declines to 1% of the value at the surface) . To calculate the diffuse attenuation coefficient for PAR (K_{par}) and optical depth (its reciprocal), we first estimated the euphotic zone (Z_e) as a function of the total pigment concentration integrated over the euphotic zone (C_{tot}) (Morel, 1988, equation 3).

$$C_{tot} = 4,910\, Z_e^{-1.34} \quad (1)$$

Equation (1) can be rearranged to solve for Z_e:

$$Z_e = e^{[(\ln Ctot - \ln 4910)/-1.34]} \quad (2)$$

where e is Euler's constant. The value of K_{par} was then calculated using (Morel, 1988, equation 4):

$$K_{par} = -\ln 0.01/Z_e = 4.605/Z_e \quad (3)$$

Given K_{par} (and its reciprocal, the optical length), then integrated concentrations could also be calculated over the top optical depth. To estimate the homogeneity line for the plots of euphotic integrals versus top optical depth integral, the line had a slope of 4.605. For plots of the integral euphotic concentration versus absolute surface concentration, it was not possible to draw a homogeneity line because the surface concentration (in units of m^{-3}) was not scaled to K_{par}.

The best fit power equation to predict the dependent variable, Y (integrated concentration) from the independent variable, X (either the discrete surface concentration in units of m^{-3} or the concentration integrated over the top optical depth, in units of m^{-2}), uses a power function:

$$\log Y = \log C + \exp(\log X) \quad (4)$$

where the constant (C) and exponent (exp) were statistically derived using least squares fit criteria. For the 100 m depth integral versus surface concentration plots, the homogeneity line was defined as when the exponent was 1, and the constant was 100 m^{-1}. For the plots of euphotic zone integrals versus the integrated concentration over the top optical depth, the homogeneity line was defined as when the exponent was 1 and the constant was 4.605 (value derived from equation (3)). Station profiles were defined as being homogeneous when they were within 10% of the homogeneity line. When the integral concentration was greater than 110% of the homogeneity line, then the vertical distribution was considered to be biased to subsurface populations (i.e., a maximum below the surface (or top optical depth). If the integral concentration was less than 90% of the homogeneity line, then the vertical profile was considered to be biased to the surface waters (or top optical depth).

The reader should note that regarding the depth integrals, for completeness, we also performed this analysis for 50 m, 150 m, and 200 m integrals but here only report the 100 m integrations as they provide the closest coefficients to the euphotic integrations across all the stations (oligotrophic, mesotrophic, and eutrophic environments).

3. Results

3.1. Global Trends for Vertical Distributions of Biogeochemical Variables Over the Top 100 m

For all variables examined (100 m integrals of chlorophyll, PIC, coccolithophore cells and aggregates, detached coccoliths, POC, and BSi), the exponents were all significantly less than 1.0 (Figure 2 and Table 2). The exponent for the fit between 100 m integrated chlorophyll versus surface chlorophyll was 0.727(±0.022), significantly lower than 1.0. Henceforth, error estimates are given in parentheses as standard errors about the mean. Moreover, for the comparison of different statistically-fit coefficients, the Z test was used to test whether differences were significant at an alpha level of 0.05 (for the two-tailed distribution and large sample size with degrees of freedom varied between 302 and 580) (Sprinthall, 2011). The integrated chlorophyll concentration at a surface chlorophyll concentration of 1.0 mg m^{-3} was 85.8(±4.301) mg m^{-2}. This was significantly lower than the value expected for a homogeneous water column (where a surface concentration of 1 mg m^{-3} would have a 100 m integral concentration of 100 mg m^{-2}). The results indicate, as expected, that in eutrophic, elevated-chlorophyll situations (above an average threshold for surface chlorophyll a of 0.57 mg m^{-3}), surface peaks in chlorophyll dominated whereas as surface chlorophyll decreases below that threshold, the profiles shift to show subsurface chlorophyll maxima.

The 100 m integrated PIC and surface concentrations also showed the tendency for subsurface peaks in low PIC regions, with a significantly lower exponent than 1 (0.560(±0.025)) than observed for the above chlorophyll distributions (Figure 2a and Table 2). Moreover, the overall data distribution is more evenly distributed on either side of the "homogeneity line" than for chlorophyll, indicating approximately equal numbers of stations characterized by a surface peak versus subsurface peak. The constant, C, in equation (1) was 40.55(±2.52) mmol m^{-2} and represents the average integrated concentration when surface PIC is 1 mmol m^{-3}. (Such an integrated PIC concentration is significantly lower than that expected for a

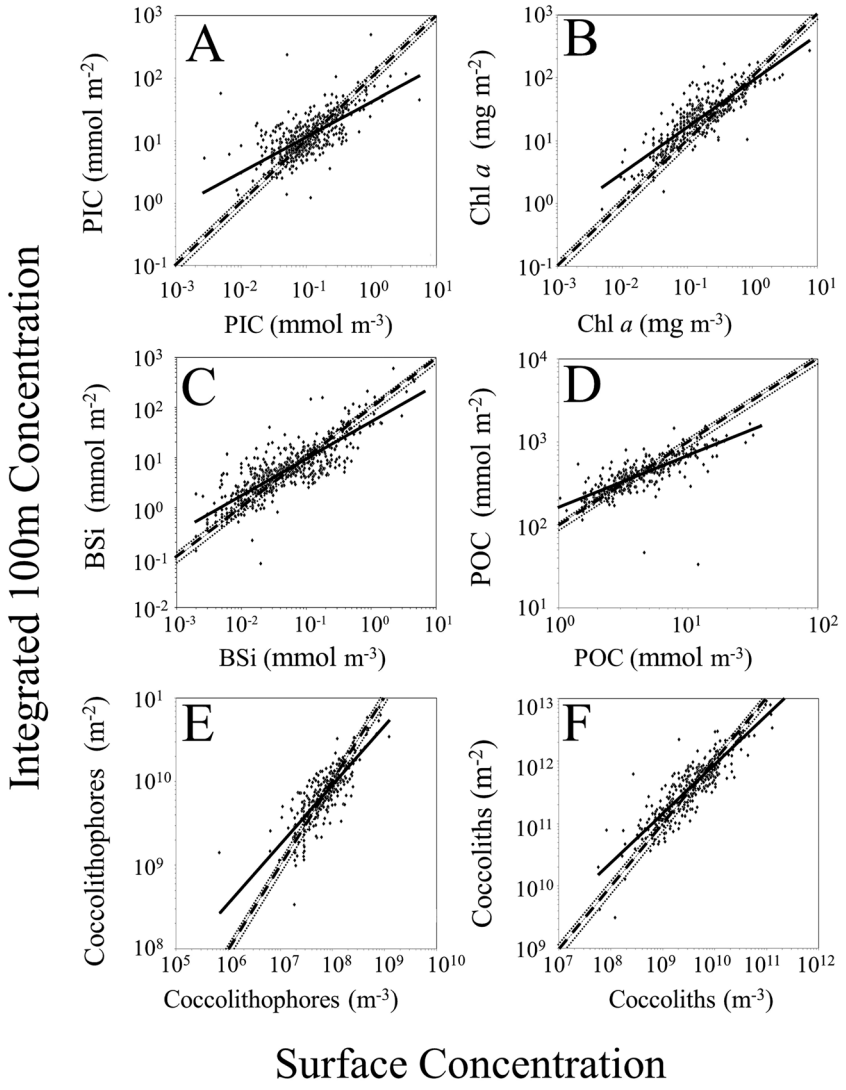

Figure 2. Concentration of biogeochemical variables (integrated to 100 m) versus their surface concentration (in the top 10 m of the water column). The dashed line represents a hypothetical homogeneous distribution of each variable (with a slope of 100 m^{-1}). The thin dotted line above and below the dashed line designates the ±10% range around the homogeneous distribution. The least squares power fit to the data is shown with the solid line. The best fit power equation coefficients are shown in Table 2.

homogenously mixed suspension of 100 mmol m^{-3}). Note, for reference, at a surface PIC concentration of 1 mmol m^{-3}, the coccolithophores would be at bloom levels and the water would be visibly brighter to the naked eye (Balch et al., 1991). Finally, regions with surface PIC concentrations lower than a threshold of 0.13 mmol m^{-3} are more likely to show a subsurface PIC peak than for regions with higher surface PIC concentrations.

The 100 m integrated coccolithophore concentration (unit: particles m^{-2}) versus surface concentrations of coccolithophore cells and aggregates (unit: particles m^{-3}) again showed a highly significant power relationship (Figure 2e and Table 2), fairly well distributed on either side of the homogeneity line. The exponent of the best fit line (0.708(±0.028)) was significantly lower than 1.0 and higher than the PIC exponent (0.560(±0.025)). The constant for the power-fit was 3.485×10^8 ($\pm 0.425 \times 10^8$) cells m^{-2} (which would be the integrated concentration where the surface concentration is equal to 10^6 particles m^{-3} (1 particle mL^{-1}; extremely low) . The threshold surface coccolithophore concentration below which subsurface peaks are observed is 0.719×10^6 cells m^{-3}.

Table 2
Least Squares Fit Coefficients for Power Equations Shown in Figures 2–4 With Standard Errors for the Exponent and Constant, Plus r^2, Degrees of Freedom (d.f.), and F Statistic (F_{stat})

	Dependent variable (100 m integrated concentration (per m^{-2}))									
Independent variable	RMS error (log units)	Exp	±	Const.	±	r^2	d.f.	Fstat	$P<$	Threshold conc. (surface; m^{-3})
Surface concentration (m^{-3})										
Biogenic silica (mmol m^{-3})	0.288	0.737	0.019	50.165	3.24	0.712	580	1433	0.001	7.26×10^{-2}
Chlorophyll *a* (mg m^{-3})	0.211	0.727	0.022	85.852	4.30	0.731	394	1072	0.001	0.57
Cocco. cells and aggregates (m^{-3})	0.196	0.708	0.028	3.485×10^{8a}	42.46	0.675	302	626	0.001	7.19×10^{7}
Coccoliths (m^{-3})	0.224	0.786	0.021	6.302×10^{8a}	108.00	0.804	353	1452	0.001	5.38×10^{9}
POC (mmol m^{-3})	0.141	0.617	0.028	164.376	7.16	0.588	341	486	0.001	3.66
PIC (mmol m^{-3})	0.233	0.560	0.025	40.555	2.52	0.482	550	512	0.001	0.13
Surface concentration	Dependent variable (euphotic integrated concentration (per m^{-2}))									
Biogenic Silica (mmol m^{-3})	0.263	0.736	0.018	28.79	1.39	0.766	478	1654	0.001	
Chlorophyll *a* (mg m^{-3})	0.198	0.534	0.017	33.576	1.04	0.661	528	1029	0.001	
Cocco. cells and aggregates (m^{-3})	0.242	0.766	0.026	1.395×10^{8b}	16.94	0.725	321	845	0.001	
Coccoliths (m^{-3})	0.266	0.816	0.018	2.475×10^{8b}	37.92	0.855	350	2071	0.001	
POC (mmol m^{-3})	0.165	0.474	0.026	133.24	6.84	0.510	317	331	0.001	
PIC (mmol m^{-3})	0.277	0.571	0.025	23.717	1.39	0.526	480	532	0.001	
Concentration in top optical depth	Dependent variable (euphotic-integrated concentration (per m^{-2}))									(m^{-2} (top opt. depth)$^{-1}$)
Biogenic Silica (mmol m^{-2} (opt. depth)$^{-1}$)	0.29	0.875	0.025	3.533	0.119	0.722	474	1228	0.001	0.12
Chlorophyll *a* (mg m^{-2} (opt. depth)$^{-1}$)	0.233	0.615	0.034	7.1172	0.33	0.439	524	411	0.001	3.10
Cocco. cells and aggregates (m^{-2} (opt. depth)$^{-1}$)	0.248	0.807	0.029	1.376×10^{7c}	2.93	0.703	318	754	0.001	2.90×10^{8}
Coccoliths (m^{-2} (opt. depth)$^{-1}$)	0.271	0.866	0.020	1.609×10^{7c}	3.56	0.848	347	1936	0.001	1.15×10^{10}
POC (mmol m^{-2} (opt. depth)$^{-1}$)	0.184	0.556	0.015	25.669	4.87	0.363	314	179	0.001	47.92
PIC (mmol m^{-2} (opt. depth)$^{-1}$)	0.291	0.566	0.027	4.9896	0.18	0.469	476	421	0.001	1.20

Note. All statistical fits showed a two-tailed alpha error with $P < 0.001$. The threshold concentration where the least squares fit line crosses the homogeneity line is given (i.e., when a homogeneity line could be calculated as in Figures 2 and 4). Below the threshold surface concentration, the vertical profiles showed statistical bias to deep subsurface maxima, while above the threshold concentration, the vertical profiles show evidence of surface maxima.
[a]Original counts and statistics were done in units per mL and subsequently converted to concentrations in units of m^{-3} to be consistent with Figure 2. Thus, as presented here, these constants represent the integrated particle concentrations (m^{-2}) at a surface concentration of 1 million particles m^{-3}. [b]Original counts and statistics were done in units per mL and subsequently converted to concentrations in units of m^{-3} to be consistent with Figure 3. Thus, as presented here, these constants represent the euphotic-integrated particle concentrations (m^{-2}) when the surface water contains 1 million particles m^{-3}. [c]Original counts and statistics were done in units per mL and subsequently converted to concentrations in units of m^{-3} to be consistent with Figure 4. Thus, as presented here, these constants represent the euphotic-integrated particle concentrations (m^{-2}) when the top optical depth contains 1 million particles m^{-2}.

We examined the microscopic-derived concentration of birefringent coccoliths in surface and 100 m integrated water columns. The exponent on this relationship (0.786(±0.021)) (Figure 2f and Table 2) was again significantly less than 1.0 but slightly greater than the exponent for the abundance of birefringent coccolithophore cells and aggregates (Figure 4). The constant was 6.30×10^8 ($\pm 1.08 \times 10^8$) coccoliths m^{-2}, which is the 100 m integrated concentration when the surface concentration is 1×10^6 coccoliths m^{-3} (or 1 mL^{-1}). The threshold surface coccolith concentration below which subsurface peaks are the norm is 5.38×10^9 coccoliths m^{-3}.

The concentration of particulate organic carbon for 100 m integrals versus surface concentrations had an exponent of 0.617 (±0.028), again significantly lower than 1.0, suggesting a tendency to form subsurface maxima in waters with low surface POC concentrations, as waters become more oligotrophic. Moreover, it is not significantly different from the exponent for PIC (Figure 3; 0.560(±0.025)). The constant, *C*, in equation (3) was 164.4 mmol m^{-2}, representing the average 100 m integrated POC concentration when surface POC is 1 mmol m^{-3}, observed at the oligotrophic extreme of the data distribution (Figure 2d). The threshold surface POC concentration below which subsurface POC maxima become the norm is 3.66 mmol POC m^{-3} (Table 2).

A plot of integrated BSi in the upper 100 m against surface BSi showed an exponent 0.737 (±0.019), almost as high as the power fit for detached coccoliths (see above), still significantly less than 1.0. Thus, BSi (and detached coccoliths) show the tendency to form subsurface maxima but these came closest to approaching a homogeneous distribution of all the variables examined here, and the r^2 for the power fit was 0.71. The

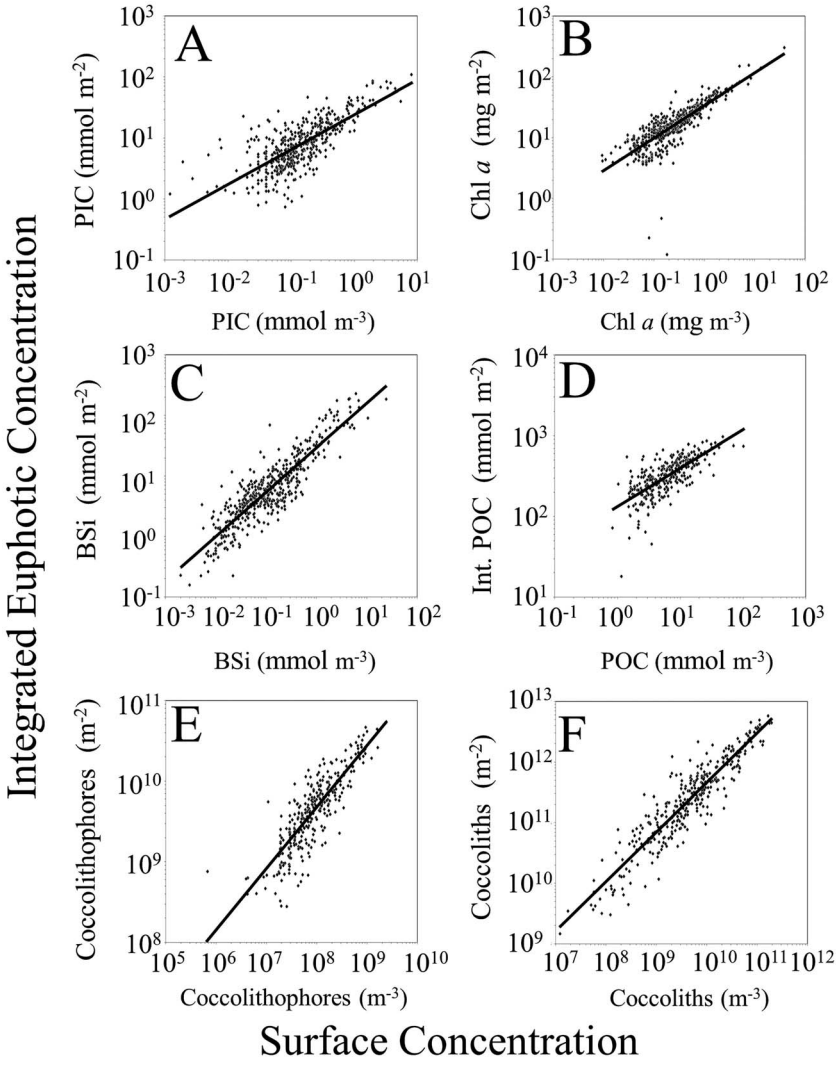

Figure 3. Concentration of biogeochemical variables (integrated over the euphotic zone) versus their surface concentration (in the top 10 m of the water column). The least squares power fit to the data is shown with the solid line. The best fit power equation coefficients are shown in Table 2.

constant, *C*, in equation (4) for BSi was 72.54 mmol m^{-2} (the average integrated concentration when surface BSi is 1 mmol m^{-3}), observed near the upper end of the data distribution shown in Figure 2c. The threshold surface BSi concentration below which subsurface BSi maxima tend to form is 7.26×10^{-2} mmol m^{-3} (i.e., 72.6 nM).

3.2. Global Trends for Vertical Distributions of Biogeochemical Variables Integrated Over the Euphotic Zone

Overall, plots of euphotic zone integrals versus the respective surface concentration (m^{-3}) showed moderate-to-strong relationships (r^2) of 0.51 to 0.85 (Figure 3 and Table 2), and with similar trends to the 100 m integrals above (Figure 2. However, euphotic zone coccolithophores were slightly more predictable from their surface concentrations than the 100 m integrals ($r^2 = 0.72$ versus 0.68, respectively) and their exponents were not significantly different.

Note that for these depictions of the data, however, it was not possible to define a homogeneity line since the euphotic zone integrals were scaled by the diffuse attenuation of PAR whereas the surface concentrations were not. In other words, in order to draw a homogeneity line, one would have to know what fraction of the euphotic zone was represented by the top meter of the water column. This would have varied for every station. The other trend for the euphotic zone integrals versus the surface concentration plots was that for the

least squares fits, constants were significantly lower than for the 100 m integrals but the exponents, on average, only differed by 8.8% (Table 2).

The power function relating the euphotic PIC concentration to the surface PIC concentration had an exponent of 0.571(±0.025) and constant of 23.72(±1.39) (where the constant in these log-log relationships signifies the euphotic integral when the surface concentration of PIC was 1 mmol m^{-3}, a relatively high PIC concentration). The r^2 value for the PIC relationship was 0.53, almost the lowest explained-variance of all the variables plotted in this fashion, yet the explained variance for predicting euphotic PIC was higher than for 100 m integrated PIC. The function relating surface chlorophyll *a* concentration to euphotic-integrated chlorophyll had an exponent of 0.534(±0.017), constant of 33.58(±1.04) and explained variance (r^2) of 0.66 (Table 2). The predictability of euphotic-integrated chlorophyll was slightly less than for 100 m integrated chlorophyll. The function relating surface BSi to euphotic zone-integrated BSi concentration showed an exponent of 0.736(±0.018), not significantly different from the 100 m integral. The explained variance for BSi (r^2 of 0.77) was slightly higher than for the 100 m integrals. Euphotic zone POC was the least predictable integral in this category based on surface concentrations, with r^2 less than for the 100 m integrated POC (r^2 = 0.51 versus 0.59, for euphotic and 100 m integrals, respectively). The exponent for the euphotic POC versus surface POC power function was 0.474(±0.026), lower than the exponent for the 100 m integral. Euphotic zone-integrated coccolith concentration was slightly more predictable from the surface concentration than the 100 m integrated concentration was (r^2 = 0.86 versus 0.80, respectively) and the exponents were not significantly different but the constant for the euphotic integral power function was significantly different, less than half of the constant in the equation for the 100 m integral (Table 2).

Given that ocean color satellites observe materials significantly weighted to the top optical depth (Gordon & McCluney, 1975), we also examined the relationships between the euphotic-integrated concentrations of the various biogeochemical properties versus the concentrations integrated over the top optical depth of the water column (Figure 4). By plotting in this fashion, we could calculate a homogeneity line (since both dependent and independent variables were scaled to optical depth). As with the other data depictions, BSi and coccolith abundance had the highest exponent in the least squares power fit. PIC and POC had the lowest exponents, approximately similar to the other data depictions while coccolithophore abundance had intermediate exponents as in all other depictions (Figure 4 and Table 2). The power function relating the euphotic PIC concentration to the top optical depth-integrated PIC concentration had an exponent of 0.566(±0.027) and constant of 4.99(±0.18). The r^2 of total euphotic-integrated PIC versus the PIC integrated over the top optical depth was lower than for the prediction based on absolute surface concentration and still at the low range of all the biogeochemical variables examined in this study. The threshold surface PIC concentration below which vertical profiles showed a statistical tendency to form subsurface maxima was 1.2 mmol m^{-2} (optical depth)$^{-1}$. BSi, on the other hand, was the moderately predictable (r^2 = 0.72) with exponent only slightly lower than 1 (0.875(±0.025)). The threshold surface BSi concentration below which vertical profiles showed significant trends to form subsurface BSi maxima was 0.12 mmol m^{-2} (optical depth)$^{-1}$. Euphotic chlorophyll *a* concentration was least predictable based on integrated chlorophyll in the top optical depth (r^2 = 0.44) rather than when it was calculated from the surface concentration (r^2 = 0.66). The 100 m integrated chlorophyll showed the highest predictability from the surface concentration (r^2 = 0.73). The threshold surface chlorophyll *a* concentration below which euphotic zone vertical profiles were statistically biased to form subsurface chlorophyll maxima was 3.1 mg m^{-2} (optical depth)$^{-1}$. For POC and PIC, the surface threshold concentrations below which the vertical profiles showed statistical trends to form subsurface maxima were 47.92 and 1.2 mmol m^{-2} (optical depth)$^{-1}$, respectively (Table 2).

3.3. Global Trends for Vertical Distributions of Biogeochemical Variables Over the Top 100 m

Regardless of how the integrals were performed (over the top 100 m or over the euphotic zone), when the integrals were plotted against the surface concentration (or concentration in the top optical depth), without exception, there was a trend of higher exponents of the least squares power functions, associated with higher coefficient of determination between integrated and surface concentration for all biogeochemical variables. In other words, variables with the highest exponents (e.g., coccolith abundance) were associated with the most explained variance and variables with the lowest exponent fits (e.g., POC or PIC) had the lowest explained variance (Figure 5). The rank order of the different biogeochemical variables showed similar (but not identical) ordering regardless of whether the integrals were estimated over the euphotic zone or over

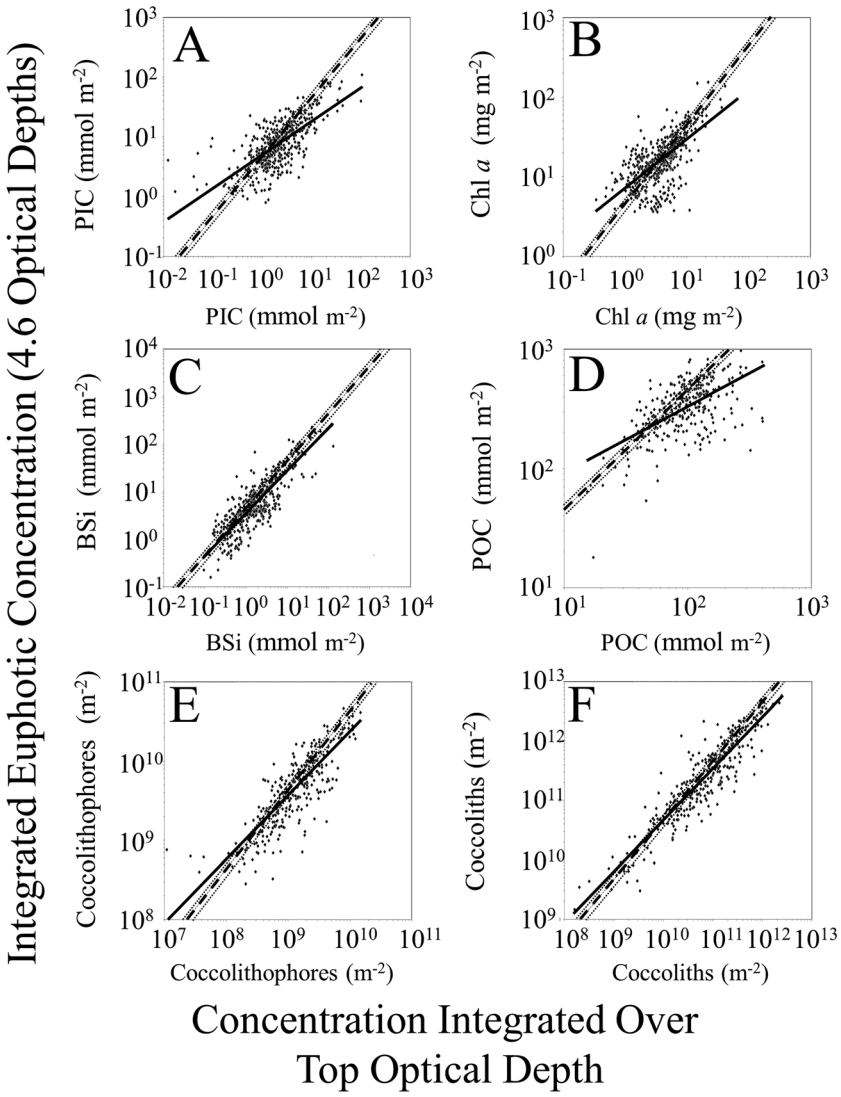

Figure 4. Concentration of biogeochemical variables (integrated over the euphotic zone; top 4.6 optical depths) versus their concentration integrated over the top optical depth). The dashed line represents a hypothetical homogeneous distribution of each variable (with a slope of 4.605). The thin dotted line above and below the dashed line designates the ±10% range around the homogeneous distribution. The least squares power fit to the data is shown with the solid line. The best fit power equation coefficients are shown in Table 2.

the top 100 m (Table 3). This trend was strongest for plots of surface concentrations versus values integrated over the top 100 m (Figure 2) followed closely by the results for surface concentration versus integrated euphotic zone concentrations (Figure 3) followed by the results for top optical depth integrals versus integrated euphotic zone concentrations (Figure 4).

4. Discussion

4.1. Vertical Distributions of Biogeochemical Variables Along a Eutrophic-to-Oligotrophic Continuum

The results presented here suggest that there are globally valid relationships between the surface (or top optical depth) concentrations of various biogeochemical variables and their euphotic zone integrals (or 100 m integrals) that cover a wide continuum of environments. The utility of these relationships is that for remote sensing, it is possible to predict (albeit empirically) the euphotic zone integral concentrations of a whole host of biogeochemical variables that have formerly been constrained to the top optical depth of the water column for satellite remote sensing purposes (Gordon & McCluney, 1975). Such predictive relationships are robust, and they also work for 100 m integrated water columns, despite the fact that in oligotrophic

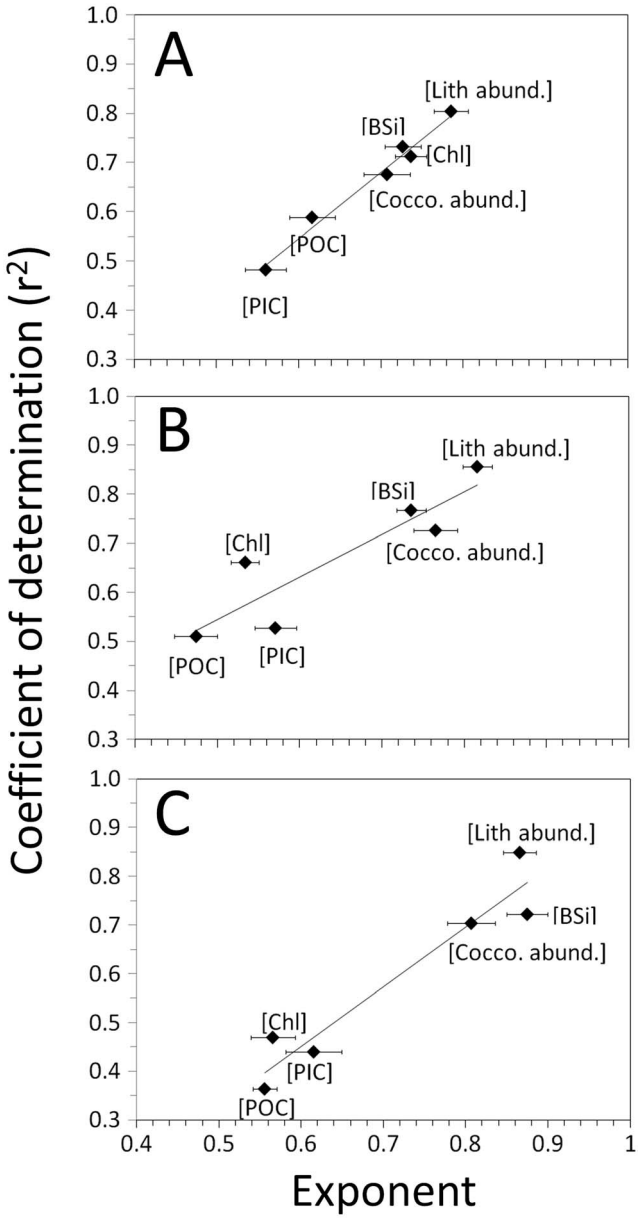

Figure 5. Coefficient of determination (r^2) for the relationships between the exponents of the various least squares-fit relationships between surface concentrations versus their integrated quantities shown in (a) Figure 2 (surface concentration (m^{-3}) versus 100 m integrated concentration), (b) Figure 3 (surface concentration (m^{-3}) versus euphotic-integrated concentration), and (c) Figure 4 (concentration integrated over top optical depth (m^{-2}) versus euphotic zone integrated concentration) The error bars reflect the standard errors of the derived exponent in the respective power functions. The statistics of the least squares fits shown in the panels are given in Table 3.

regions, the a 100 m water column will not include deepest parts of the euphotic zone, and in eutrophic regions, the 100 m water column will include both the euphotic zone and parts of the aphotic zone.

This is not the first time that integrated chlorophyll *a* has been projected from surface measurements. As noted in the introduction, others have provided statistical means to estimate the euphotic concentration of chlorophyll *a* based on satellite-derived, surface chlorophyll in the top optical depth (Balch et al., 1992; Morel, 1988; Platt et al., 1988; Platt & Herman, 1983). However, the results presented here (Figures 2–4) demonstrate for the first time that euphotic zone-integrated concentrations of coccolithophores (concentration of plated cells or their detached coccoliths) as well as biogeochemical variables of PIC, POC, and BSi, spanning orders of magnitude can also be predicted across oligotrophic, mesotrophic, and eutrophic environments.

Moreover, the explained variance by these various relationships between the integrated versus surface concentration increases as the exponent approaches 1.0, which might logically be expected. For example, when 100 m or euphotic concentrations approach a homogeneous distribution, then their predictability from surface concentrations increases. Alternatively, as deep maxima develop in stratified environments, and populations become more isolated from the surface, the exponent of the relationships (statistically fit slopes in Figures 2–4 and Table 2) decreases further, and the ability to predict integrated properties from surface concentrations degrades (Figure 5). While the trends are not particularly surprising, what is surprising is how well-defined this relationship between the exponent and the explained-variance is for six diverse biogeochemical variables. The variables that can be associated with multiple taxa (such as chlorophyll *a*, PIC, and POC) are the least predictable, whereas biogeochemical variables associated with a single algal class (coccolithophorids or diatoms, excluding the contributions of relatively rare foraminifera or pteropods to PIC and relatively rare radiolarians to the BSi concentration). POC also includes a large fraction of detrital material (Passow, 2002), which likely also contributes to its lower exponent and lower overall predictability across the global ocean.

4.2. Vertical Distributions of Coccolithophores and PIC Do Not Match

The above-noted difference between the exponents for integrated versus surface properties for coccolithophore abundance or PIC concentration suggests that the observed PIC is not just from coccolithophores but is originating from other calcium carbonate particles not identified as coccolithophores in our CCC image analysis software (Balch & Utgoff, 2009). This conclusion is buttressed by the relationship between integrated PIC versus the concentration of detached and attached coccoliths (Figure 6; where "attached coccoliths" is defined as the coccolithophore concentration multiplied by 15, derived from the coccolithophore species, *E. huxleyi*) (Balch et al., 1993). Note that this value of 15 is conservative as it is the minimum number of coccoliths per cell for 112 species for a wide range of coccolithophore species (Boeckel & Baumann, 2008) (whereas the maximum number of coccoliths per cell can exceed ~100 depending on the species). As noted above, a conservative assumption of 15 coccoliths per plated cell is reasonable for *E. huxleyi* cells in culture (Balch et al., 1993) and in the field in *E. huxleyi* blooms, as observed by Balch et al. (2011) and Balch et al. (2000). Poulton et al. (2011) found that ratios of detached coccoliths per plated *E. huxleyi* cell to double this amount over the Patagonian Shelf, which included a turbid coccolithophore bloom of *E. huxleyi* (31.05 ± 4.34 coccoliths per coccosphere; see their Table 2; note that one

Table 3
Summary of the Statistics for Each Relationship Described in Figure 5

Dependent variable	Independent variable	RMS error *Y*	Slope	±	Const.	±	r^2	d.f.	F_{stat}	*P*<
100 m integrated conc. (m^{-2})	Surface conc. (m^{-3})	0.0183	1.349	0.098	−0.264	0.068	0.980	4	191.2	0.001
Euphotic integrated conc. (m^{-2})	Surface conc. (m^{-3})	0.0675	0.868	0.214	0.110	0.142	0.804	4	16.4	0.02
Euphotic integrated conc. (m^{-2})	Conc. in top optical depth (m^{-2})	0.0612	1.222	0.181	−0.282	0.132	0.919	4	45.6	0.001

Note. The two-tailed significance probability is given in the right-most column.

quarter of the stations in that table were dominated by species other than *E. huxleyi*). Nonetheless, this conservative value of coccoliths per cell translates roughly to a PIC per coccolith between 0.066 and 0.0046 pmol coccolith^{-1} (or 0.8 and 0.05 pg PIC coccolith^{-1}, respectively, a total range of 16-fold). Typical values of the PIC per coccolith for the ubiquitous coccolithophore *E. huxleyi* fall between 0.2 and 0.9 pg coccolith (Balch, 1991; Balch et al., 1991; Poulton et al., 2011), in reasonable agreement with the values seen in our global data set (Figure 6). Coccolith content estimates exist for a few other species (e.g., see Young & Ziveri, 2000, and references therein). Young and Ziveri (2000) suggest that the average mass for small coccoliths is 2.6 pg $CaCO_3$ coccolith^{-1} (=0.31 pg PIC coccolith^{-1} = 0.026 pmol PIC coccolith^{-1}; see their Table 2). Our results (Figure 6) suggest that for samples with highest coccolithophore abundance, the coccolith mass fell primarily between the 0.0083 and 0.0166 pmol PIC (0.1–0.2 pg PIC coccolith^{-1}, respectively) with the mean value of 0.013 pmol PIC coccolith^{-1} (= 0.156 pg PIC coccolith^{-1}). This value is about half the value of Young and Ziveri (2000). Nonetheless, we saw another group of stations with coccolith PIC values of 0.033–0.066 pmol coccolith^{-1} (=0.4–0.8 pg coccolith^{-1}), values that fell within the range of some of the moderately sized coccoliths described by Young and Ziveri (2000). Such variability in these PIC coccolith^{-1} values has been observed in field measurements from other parts of the world ocean, too (Balch et al., 2000).

There are multiple causes of this high overall variability. Even within *E. huxleyi*, various morphotypes can account for sixfold variation in PIC content (Poulton et al., 2011). Also, the presence of other calcite particles that are not counted in our birefringent coccolith counts could be raising the overall PIC concentration without an increase in the coccolithophore or coccolith concentration. An example of this are the recently described, previously unidentified, marine biogenic $CaCO_3$ particles produced by bacteria or associated with marine polymeric substances, for which the PIC concentration can actually surpass that of coccolithophores. Their abundance varies from undetectable to 150 particles mL^{-1} with an average of 30 particles mL^{-1}.(Heldal et al., 2012). Such particles would raise our PIC per coccolith to values exceeding maximum values found in coccolithophore cultures. Moreover, large coccolithophore species, such as *Coccolithus pelagicus*, have coccolith masses an order of magnitude greater than for *E. huxleyi* (Young & Ziveri, 2000), which could also significantly raise the PIC per coccolith.

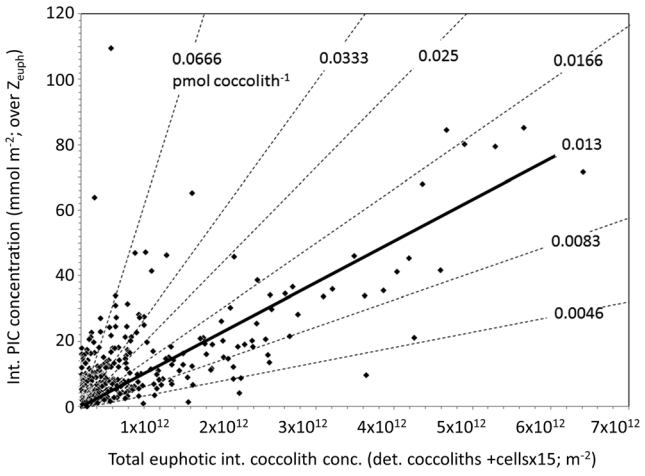

Figure 6. Plot of euphotic zone-integrated PIC concentration (mmol m^{-2}) versus total euphotic-integrated coccolith concentration (per $m^{-2)}$. The integrated coccolith concentration makes the simplifying assumption that each coccolithophore cell, regardless of species, has 15 coccoliths surrounding it. The heavy black line is the least squares fit to the data. The equation for the line is Y(±12.03) = 1.26 × 10^{-11} (±5.26 × 10^{-13})X, degree of freedom (d.f.) = 342, r^2 = 0.628, F_{stat} = 578, and $P < 0.001$. The values in parentheses are the standard error associated with each fit term. The dashed lines represent isopleths in units of picomoles PIC per coccolith. From highest to lowest PIC content, the values equate to 0.8, 0.4, 0.3, 0.2, 0.1, and 0.05 pg PIC per coccolith. The slope of the heavy, least square fit line translates to 0.156 pgPIC per coccolith.

Moreover, if there were any significant dissolution of PIC happening in the upper 100 m or euphotic zone (but not at the surface or top optical depth), then this would drive the slope of the data distributions in Figures 2 and 4 toward (or below) the homogeneity line, such that distributions would be biased to the surface waters. Clearly, for both PIC, coccolithophore abundance, and coccolith abundance, there are significant numbers of data that fall below the homogeneity line (Figures 2 and 4). However, the majority of the data show that for BSi, PIC, plated coccolithophores, detached coccoliths, and POC, the measured euphotic-integrated concentrations are less than 90% of the homogeneity line, suggesting a surface bias to their vertical distribution (Table 4). Only chlorophyll

Table 4
Summary for Global Station Comparison of Surface and Integrated Euphotic Profiles

Heterogeneous versus homogeneous criterion	BSi	PIC	Plated cells ± agg	Coccoliths	POC	Chl
Variable is biased to top OD (where integral euphotic conc. <90% of the top OD × 4.6)	60.5%	59.2%	60.9%	54.2%	60.1%	46.4%
Variable is biased to below the top OD (where integral euphotic conc. >110% of the top OD × 4.6)	25.6%	29.9%	22.5%	29.8%	19.6%	37.5%
Variable is homogeneous (where integral euphotic conc. >90% and <110% of top OD value × 4.6)	13.9%	10.9%	16.6%	16.0%	20.3%	16.2%
Total percentage	100.0%	100.0%	100.0%	100.0%	100.0%	100.0%
Number of stations	476	478	320	349	316	526

Note. The criterion for a homogeneous distribution was when the integral concentration was >90% and <110% of the concentration in the top optical depth × 4.6 (assumes that the euphotic zone extends to the 1% light level). A surface bias was defined as when the integral concentration was <90% of the surface value times 4.6. A subsurface bias was defined as when the integral concentration was >110% of the surface concentration times 4.6.

concentration shows a minority of stations biased to the top optical depth, with the majority of data either falling along the homogeneity line or showing a subsurface bias (in agreement with Figure 6 of Balch et al., 1992). We calculated these statistics for the euphotic integrals only, not the 100 m integrals (as mentioned earlier), since 100 m integrals would not cover the entire euphotic zone in oligotrophic subtropical gyres and they would likely include aphotic depths in the more eutrophic regions. This is less of an issue when the integrated quantities are optically scaled to the euphotic zone.

4.3. Water Column Stability and Phytoplankton Abundance

The results of these cruises offer an ideal opportunity to examine the fundamental effect of water column stability on the distribution and concentrations of different bulk biogeochemical properties (PIC, chlorophyll, POC, and BSi) plus coccolithophore and coccolith abundance, across the many different ecological domains sampled during these global cruises. Margalef (1978), in his seminal paper, addressed the impact of turbulence and nutrients on the life forms of the nanoplankton and microplankton (diatoms, coccolithophores, and dinoflagellates) (no picophytoplankton were included, nor, indeed known, at the time his paper was published). His conceptual model listed diatoms associated with well-mixed, high nutrient environments and coccolithophores as growing optimally in environments of intermediate turbulence and nutrients. We calculated the Brunt-Väisälä Frequency (BVF) at the base of the euphotic zone to estimate stratification there, which would affect the upward diffusion of potentially limiting nutrients.

While the vertical sections of various properties showed little correspondence with BVF (results not shown), the plotting of the integral euphotic properties versus the BVF at the base of the euphotic zone showed similar trends for PIC, coccolithophore abundance, and coccolith abundance (Figure 7); that is, the euphotic-integrated PIC, coccolithophores, and detached coccoliths showed highest range in concentrations in moderately stratified environments, when the BVF at the base of the euphotic zone was 5–10 cycles h^{-1} (Figure 7). Temporally, the spring diatom bloom (which occurs in high-nutrient, high turbulence conditions) often precedes the spring coccolithophore bloom (as the water column stratifies and nutrients decrease) (Boyd et al., 2010; Leblanc et al., 2009), in agreement with Margalef (1978). Moreover, there are major ocean regions where phytoplankton (as chlorophyll) and coccolithophores (as PIC) peak sequentially in time (Hopkins et al., 2015), in a Margalef-like succession, particularly in shelf regions and upwelling areas. This is contrasted with open ocean areas, which show a coexistence-type phenology (Hopkins et al., 2015). We, too, found widely variable results in this study in which coccolithophore abundance sometimes showed enhanced integral concentrations in moderately stratified environments but other times with little-to-no enhancement. However, while not as strong, trends in chlorophyll (representative of all phytoplankton) also showed cases with highest values at moderate BVFs more consistent with the concept of a "rising tide lifts all phytoplankton" (Barber & Hiscock, 2006). Moreover, there were an equal number of cases where phytoplankton did not respond to BVF, suggesting that other factors besides turbulence (such as nutrient history and turbulence history) were also involved, perhaps less supportive of the Margalef-type succession, as described by Hopkins et al. (2015). It is likely that populations at these moderate BVFs were not in stable equilibrium but were constantly changing as a function of growth and grazing, typical for frontal zones (Holligan et al., 1984), which would increase the variance in the associated biogeochemical properties.

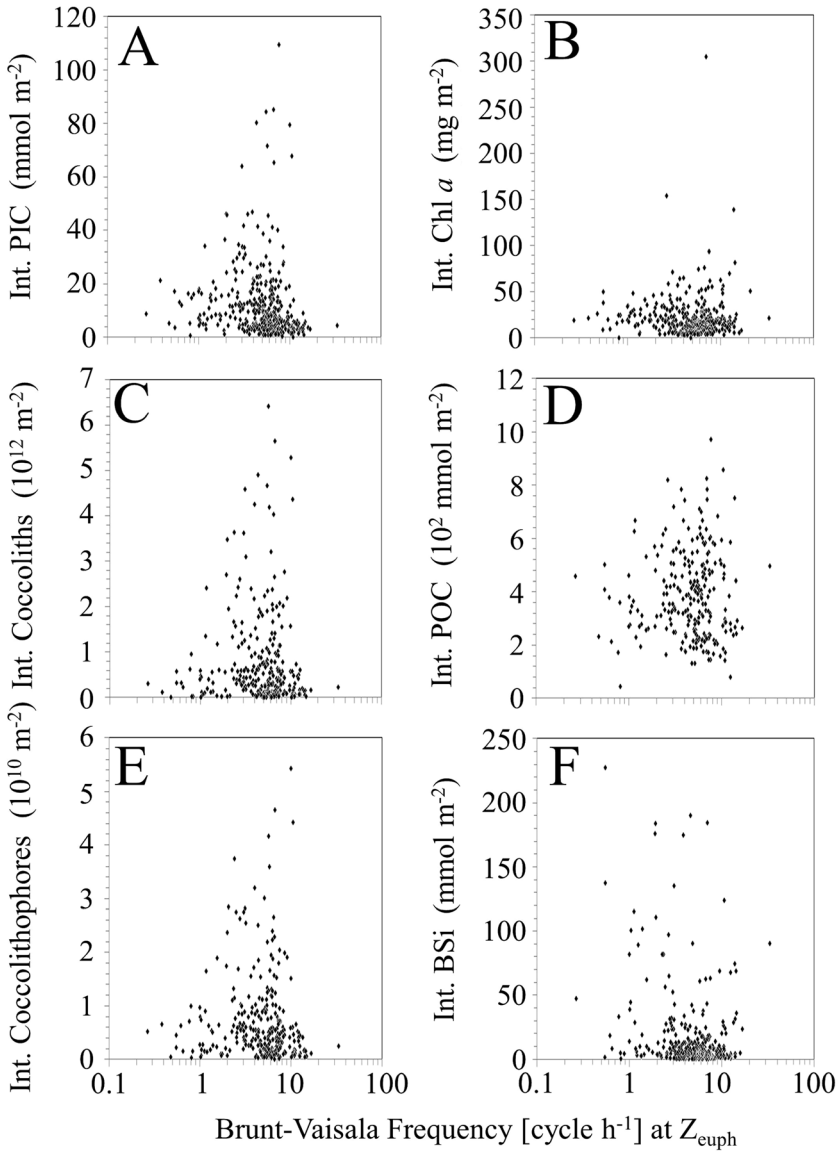

Figure 7. Plots of euphotic-zone-integrated biogeochemical variables against stratification (as Brunt-Väisälä frequency shown on log scales)). (a) PIC, (b) chlorophyll a, (c) coccolith concentration, (d) POC, (e) coccolithophore concentration, and (f) BSi.

The least responsive property that we measured was the integrated POC concentration (possibly because a significant fraction of the POC is nonliving, detrital POC). That PIC, coccolithophores, and coccoliths showed more responsiveness to BVF might suggest that they were predominantly associated with living, growing cells than POC or BSi (which could have a significant detrital fraction). The significance of this is that the biogeochemically active regions of the global ocean, which are responsible for the major export fluxes to deep waters, can be defined, even in a probabilistic way, by BVF at the base of the euphotic zone, a measurement which is easy to make from profiling floats. Such a time series of BVF would allow one to assess the potential for upward nutrient diffusion within that water mass, along with possible cause and effect for the biology to respond within the euphotic zone.

4.4. Concluding Remarks

Taken together, the results presented here demonstrate that there is wide variability in vertical profiles for different biogeochemical properties in the global ocean but there is a high degree of predictability, nonetheless. Moreover, there are satellite algorithms for most of these variables. Despite taxonomic differences in the organisms that drive each of these algorithms, we demonstrate that there is remarkable ability to predict

euphotic zone (and even 100 m)-integrated variables based on just surface observations. In this work, we have defined those relationships. Future work should focus on the implications of these differing relationships on marine ecosystems. Ultimately, these relationships promise fertile research opportunities in remote sensing and biogeochemical modeling, for estimating pelagic budgets in the sea.

Acknowledgments

Funding for W.M.B. over the years for the cruise work presented here came from the National Science Foundation (OCE-9596167, OCE-0961660, OCE-1220068, OCE-0322074 SubGrant S0993A-D, OCE-0136541, and OCE-0728582) and the National Aeronautics and Space Administration (NNX17AI77G, NNX11AO72G, NNX11AL93G, NNX14AQ41G, NNX14AQ43A, NNX14AL92G, NNX14AM77G, NNG04HZ25C, NNG04GI11G, NNX08AJ88A, NNX07AD01G, NNX10AT67G, NAGW 2426, and NAS5-31363). Data used for this paper are stored in the NASA-SEABASS data archive (http://seabass.gsfc.nasa.gov/) and BCO-DMO archive (http://www.bco-dmo.org/). We thank the Atlantic Meridional Transect program of the UK and Phil Boyd (University Tasmania) for providing us space aboard their cruises. Three anonymous reviewers provided helpful comments on a previous draft of this work. This study is a contribution to the international IMBeR project and was supported by the UK Natural Environment Research Council National Capability funding to Plymouth Marine Laboratory and the National Oceanography Centre, Southampton. This is manuscript number 321 of the Atlantic Meridional Transect Programme.

References

Balch, W. (1991). Erratum from "Biological and optical properties of mesoscale coccolithophore blooms in the Gulf of Maine" by Balch, W. M., P. M. Holligan, S. G. Ackleson and K. J. Voss. *Limnology and Oceanography*, *36*(7), 1462.

Balch, W., & Utgoff, P. (2009). Potential interactions among ocean acidification, coccolithophores and the optical properties of seawater. *Oceanography*, *22*(4), 146–159.

Balch, W. M., Bates, N. R., Lam, P. J., Twining, B. S., Rosengard, S. Z., Bowler, B. C., … Rauschenberg, S. (2016). Factors regulating the Great Calcite Belt in the Southern Ocean and its biogeochemical significance. *Global Biogeochemical Cycles*, *30*, 1124–1144. https://doi.org/10.1002/2016GB005414

Balch, W. M., Bowler, B. C., Drapeau, D. T., Poulton, A., & Holligan, P. (2010). Biominerals and the vertical flux of particulate organic carbon from the surface ocean. *Geochemical Research Letters*, *37*, L22605. https://doi.org/10.1029/2010GL044640

Balch, W. M., Drapeau, D., & Fritz, J. (2000). Monsoonal forcing of calcification in the Arabian Sea. *Deep-Sea Research Part II*, *47*, 1301–1337.

Balch, W. M., Drapeau, D. T., Bowler, B. C., & Booth, E. (2007). Prediction of pelagic calcification rates using satellite-measurements. *Deep -Sea Research II (Chapman Calcification Conference Special Volume)*, *54*, 478–495.

Balch, W. M., Evans, R., Brown, J., Feldman, G., McClain, C., & Esais, W. (1992). The remote sensing of ocean primary productivity-use of a new data compilation to test satellite algorithms. *Journal of Geophysical Research*, *97*, 2279–2293.

Balch, W. M., & Fabry, V. J. (2008). Ocean acidification: Documenting its impact on calcifying phytoplankton at basin scales. *Marine Ecology Progress Series*, *373*, 239–247.

Balch, W. M., Gordon, H. R., Bowler, B. C., Drapeau, D. T., & Booth, E. S. (2005). Calcium carbonate budgets in the surface global ocean based on MODIS data. *Journal of Geophysical Research*, *110*, C07001. https://doi.org/10.01029/02004JC002560

Balch, W. M., Holligan, P. M., Ackleson, S. G., & Voss, K. J. (1991). Biological and optical properties of mesoscale coccolithophore blooms in the Gulf of Maine. *Limnology and Oceanography*, *36*, 629–643.

Balch, W. M., Kilpatrick, K., Holligan, P. M., Harbour, D., & Fernandez, E. (1996). The 1991 coccolithophore bloom in the central north Atlantic. II. Relating optics to coccolith concentration. *Limnology and Oceanography*, *41*, 1684–1696.

Balch, W. M., Kilpatrick, K. A., & Holligan, P. M. (1993). Coccolith formation and detachment by *Emiliania huxleyi* (Prymnesiophyceae). *Journal of Phycology*, *29*, 566–575.

Balch, W. M., Poulton, A. J., Drapeau, D. T., Bowler, B. C., Windecker, L., & Booth, E. (2011). Zonal and meridional patterns of phytoplankton biomass and carbon fixation in the Equatorial Pacific Ocean, between 110°W and 140°W. *Deep-Sea Research Part II*, *58*(3–4), 400–416.

Barber, R. T., & Hiscock, M. R. (2006). A rising tide lifts all phytoplankton: Growth response of other phytoplankton taxa in diatom-dominated blooms. *Global Biogeochemical Cycles*, *20*, GB4S03. https://doi.org/10.1029/2006GB002726

Billard, C., & Inouye, I. (2004). What's new in coccolithophore biology? In H. R. Thierstein & J. R. Young (Eds.), *Coccolithophores, from molecular processes to global impact* (pp. 1–29). New York: Springer.

Boeckel, B., & Baumann, K. H. (2008). Vertical and lateral variations in coccolithophore community structure across the subtropical frontal zone in the South Atlantic Ocean. *Marine Micropaleontology*, *67*(3–4), 255–273.

Boyd, P. W., Strzepek, R., Fu, F., & Hutchins, D. A. (2010). Environmental control of open-ocean phytoplankton groups: Now and in the future. *Limnology and Oceanography*, *55*(3), 1353–1376.

Brown, C. W., & Yoder, J. A. (1994). Coccolithophorid blooms in the global ocean. *Journal of Geophysical Research*, *99*(C4), 7467–7482.

Brzezinski, M. A., & Nelson, D. M. (1989). Seasonal changes in the silicon cycle within a Gulf Stream warm-core ring. *Deep-Sea Research I*, *36*, 1009–1030.

Cheng, Z., Zheng, Y., Mortlock, R., & Van Geen, A. (2004). Rapid multi-element analysis of groundwater by high-resolution inductively coupled plasma mass spectrometry. *Analytical and Bioanalytical Chemistry*, *379*(3), 512–518.

Cullen, J. J. (1982). The deep chlorophyll maximum: Comparing vertical profiles of chlorophyll *a*. *Canadian Journal of Fisheries and Aquatic Sciences*, *39*, 791–803.

Cullen, J. J., & Eppley, R. W. (1981). Chlorophyll maximum layers of the Southern California Bight and possible mechanisms of their formulation and maintenance. *Oceanologica Acta*, *4*(1), 23–32.

Edvardsen, B., Eikrem, W., Green, J. C., Andersen, R. A., Moon-Van der Staay, S. Y., & Medlin, L. K. (2000). Phylogenetic reconstructions of the Haptophyta inferred from 18S ribosomal DNA sequences and available morphological data. *Phycologia*, *39*, 19–35.

Francois, R., Honjo, S., Krishfield, R., & Manganini, S. (2002). Factors controlling the flux of organic carbon to the bathypelagic zone of the ocean. *Global Biogeochemical Cycles*, *16*(4), 1087. https://doi.org/10.1029/2001GB001722

Freeman, N. M., & Lovenduski, N. S. (2015). Decreased calcification in the Southern Ocean over the satellite record. *Geophysical Research Letters*, *42*(6), 1834–1840. https://doi.org/10.1002/2014GL062769

Galí, M., Devred, E., Levasseur, M., Royer, S. J., & Babin, M. (2015). A remote sensing algorithm for planktonic dimethylsulfoniopropionate (DMSP) and an analysis of global patterns. *Remote Sensing of Environment*, *171*, 171–184.

Gordon, H. R., Boynton, G. C., Balch, W. M., Groom, S. B., Harbour, D. S., & Smyth, T. J. (2001). Retrieval of coccolithophore calcite concentration from SeaWiFS imagery. *Geochemical Research Letters*, *28*(8), 1587–1590.

Gordon, H. R., & McCluney, W. R. (1975). Estimation of the depth of sunlight penetration in the sea for remote sensing. *Applied Optics*, *14*, 413–416.

Haidar, A. T., & Thierstein, H. R. (2001). Coccolithophore dynamics off Bermuda (N. Atlantic). *Deep-Sea Research*, *48*(8–9), 1925–1956.

Haidar, A. T., Thierstein, H. R., & Deuser, W. G. (2000). Calcareous phytoplankton standing stocks, fluxes and accumulation in Holocene sediments off Bermuda (N. Atlantic). *Deep-Sea Research*, *47*(9–11), 1907–1938.

Heldal, M., Norland, S., Erichsen, E. S., Thingstad, T. F., & Bratbak, G. (2012). An unaccounted fraction of marine biogenic $CaCO_3$ particles. *PLoS Biology*, *7*(10), 1–6.

Holligan, P. M., Charalampopoulou, A., & Hutson, R. (2010). Seasonal distributions of the coccolithophore, *Emiliania huxleyi*, and of particulate inorganic carbon in surface waters of the Scotia Sea. *Journal of Marine Systems*, *82*(4), 195–205.

Holligan, P. M., Harris, R. P., Newell, R. C., Harbor, D. S., Head, R. N., Lindley, E. A. S., … Weekley, C. M. (1984). Vertical distribution and partitioning of organic carbon in mixed, frontal and stratified waters of the English Channel. *Marine Ecology Progress Series*, *14*, 111–127.

Holligan, P. M., Viollier, M., Harbout, D. S., Camus, P., & Champagne-Philippe, M. (1983). Satellite and ship studies of coccolithophore production along a continental shelf edge. *Nature*, *304*(5924), 339–342.

Hopkins, J., Henson, S. A., Painter, S. C., Tyrrell, T., & Poulton, A. J. (2015). Phenological characteristics of global coccolithophore blooms. *Global Biogeochemical Cycles*, *29*, 239–253. https://doi.org/10.1002/2014GB004919

JGOFS (1996). Protocols for the Joint Global Ocean Flux Study (JGOFS) core measurements. In A. Knap (Ed.), *Scientific committee on oceanic research, international council of scientific unions* (p. 170). Bergen, Norway: Intergovernmental Oceanographic Commission.

Leblanc, K., Hare, C. E., Feng, Y., Berg, G. M., DiTullio, G. R., Neeley, A., … Hutchins, D. A. (2009). Distribution of calcifying and silicifying phytoplankton in relation to environmental and biogeochemical parameters during the late stages of the 2005 North East Atlantic Spring Bloom. *Biogeosciences*, *6*, 2155–2179.

Margalef, R. (1978). Life-forms of phytoplankton as survival alternatives in an unstable environment. *Oceanologica Acta*, *1*(4), 493–509.

McIntyre, A., & Be, A. W. H. (1967). Modern coccolithophoridae of the Atlantic Ocean. I. Placoliths and cyrtoliths. *Deep-Sea Research and Oceanographic Abstracts*, *14*, 561–597.

Morel, A. (1988). Optical modeling of the upper ocean in relation to its biogenous matter content (case 1 waters). *Journal of Geophysical Research*, *93*, 10,749–10,768.

Moshkovitz, S., & Osmond, K. (1989). The optical properties and microcrystallography of *Arkhangelskiellaceae* and some other calcareous nannofossils in the Late Cretaceous. In J. A. Crux & S. E. van Heck (Eds.), *Nannofossils and their applications* (pp. 76–97). Chichester: Ellis Horwood.

Paasche, E. (1973). Silicon and the ecology of marine planktonic diatoms. 1. *Thalassiosira pseudonana* (*Cyclotella nana*) grown in chemostats with silicate as the limiting nutrient. *Marine Biology*, *19*, 117–126.

Parsons, T. R., Maita, Y., & Lalli, C. M. (1984). *A manual of chemical and biological methods for seawater analysis* (173 pp.). New York: Pergamon Press Inc.

Passow, U. (2002). Transparent exopolymer particles (TEP) in aquatic environments. *Progress in Oceanography*, *55*(3–4), 287–333.

Phinney, D. A., & Yentsch, C. S. (1985). A novel phytoplankton chlorphyll technique: Toward automated analysis. *Journal of Plankton Research*, *7*(5), 633–642.

Platt, T., & Herman, A. W. (1983). Remote sensing of phytoplankton in the sea: Surface-layer chlorophyll as an estimate of water-column chlorophyll and primary production. *International Journal of Remote Sensing*, *4*(2), 343–351.

Platt, T., Sathyendranath, S., Caverhill, C. M., & Lewis, M. R. (1988). Ocean primary production and available light: Further algorithms for remote sensing. *Deep-Sea Research*, *35*(6A), 855–879.

Poulton, A. J., Charalampopoulou, A., Young, J. R., Tarran, G. A., Lucas, M. I., & Quartly, G. D. (2010). Coccolithophore dynamics in non-bloom conditions during late summer in the central Iceland Basin (July–August 2007). *Limnology and Oceanography*, *55*(4), 1601–1613. https://doi.org/10.4319/lo.2010.1655.1604.1601

Poulton, A. J., Holligan, P. M., Charalampopoulou, A., & Adey, T. R. (2017). Coccolithophore ecology in the tropical and subtropical Atlantic Ocean: New perspectives from the Atlantic meridional transect (AMT) programme. *Progress in Oceanography*. https://doi.org/10.1016/j.pocean.2017.01.003

Poulton, A. J., Sanders, R., Holligan, P. M., Adey, T., Stinchcombe, M., Brown, L., & Chamberlain, K. (2006). Phytoplankton mineralisation in the tropical and subtropical Atlantic Ocean. *Global Biogeochemical Cycles*, *20*, GB4002. https://doi.org/10.1029/2006GB002712

Poulton, A. J., Young, J. R., Bates, N. R., & Balch, W. M. (2011). Biometry of detached *Emiliania huxleyi* coccoliths along the Patagonian Shelf. *Marine Ecology Progress Series*, *443*, 1–17.

Reid, F. (1980). Coccolithophorids of the North Pacific Central Gyre with notes on their vertical and seasonal distribution. *Micropaleontology*, *26*, 151–176.

Robertson, J. E., Robinson, C., Turner, D. R., Holligan, P., Watson, A. J., Boyd, P., … Finch, M. (1994). The impact of a coccolithophore bloom on oceanic carbon uptake in the northeast Atlantic during summer 1991. *Deep-Sea Research Part I*, *41*(2), 297–314.

Sprinthall, R. C. (2011). *Basic statistical analysis* (9th ed.). Boston, MA: Allyn & Bacon.

Stramski, D., Reynolds, R. A., Babin, M., Kaczmarek, S., Lewis, M. R., & Röttgers, R. (2008). Relationships between the surface concentration of particulate organic carbon and optical properties in the eastern South Pacific and eastern Atlantic Oceans. *Biogeosciences*, *5*, 171–201.

Strickland, J. D. H. (1968). A comparison of profiles of nutrient and chlorophyll concentrations taken from discrete depths and by continuous recording. *Limnology and Oceanography*, *13*, 388–391.

Young, J. R., & Ziveri, P. (2000). Calculation of coccolith volume and its use in calibration of carbonate flux estimates. *Deep-Sea Research Part II: Topical Studies in Oceanography*, *47*(9–11), 1679–1700.